

Article

# Catalytic Properties and Recycling of NiFe<sub>2</sub>O<sub>4</sub> Catalyst for Hydrogen Production by Supercritical Water Gasification of Eucalyptus Wood Chips

Ane Caroline Pereira Borges <sup>1</sup>, Jude Azubuike Onwudili <sup>2,\*</sup>, Heloysa Andrade <sup>1,3</sup>,  
Carine Alves <sup>1,4,5</sup>, Andrew Ingram <sup>6</sup>, Silvio Vieira de Melo <sup>1,5</sup> and Ednildo Torres <sup>1,5</sup>

- <sup>1</sup> Centro Interdisciplinar em Energia e Ambiente (CIENAM), Campus Universitário Federação/Ondina, Universidade Federal da Bahia (UFBA), Salvador 40170-115, Brazil; anecborges@gmail.com (A.C.P.B.); handrade@ufba.br (H.A.); carine.alves@ufrb.edu.br (C.A.); sabvm@ufba.br (S.V.d.M.); ednildo@ufba.br (E.T.)
  - <sup>2</sup> Energy and Bioproducts Research Institute, College of Engineering and Physical Sciences, Aston University, Birmingham B4 7ET, UK
  - <sup>3</sup> Instituto de Química, Universidade Federal da Bahia (UFBA), Campus Universitário de Ondina, Salvador 40170-290, Brazil
  - <sup>4</sup> Engenharia de Energia, Universidade Federal do Recôncavo da Bahia (UFRB), Feira de Santana 44085-132, Brazil
  - <sup>5</sup> Programa de Engenharia Industrial, Escola Politécnica, Universidade Federal da Bahia, Rua Prof. Aristides Novis, 2, 6° Andar, Federação, Salvador 40210-630, Brazil
  - <sup>6</sup> School of Chemical Engineering, University of Birmingham, Birmingham B15 2TT, UK; a.ingram@bham.ac.uk
- \* Correspondence: j.onwudili@aston.ac.uk

Received: 27 July 2020; Accepted: 28 August 2020; Published: 2 September 2020



**Abstract:** Nickel iron oxide (NiFe<sub>2</sub>O<sub>4</sub>) catalyst was prepared by the combustion reaction method and characterized by XRD, N<sub>2</sub> adsorption/desorption, thermogravimetric analysis (TG), and temperature programmed reduction (TPR). The catalyst presented a mixture of oxides, including the NiFe<sub>2</sub>O<sub>4</sub> spinel and specific surface area of 32.4 m<sup>2</sup> g<sup>-1</sup>. The effect of NiFe<sub>2</sub>O<sub>4</sub> catalyst on the supercritical water gasification (SCWG) of eucalyptus wood chips was studied in a batch reactor at 450 and 500 °C without catalyst and with 1.0 g and 2.0 g of catalyst and 2.0 g of biomass for 60 min. In addition, the recyclability of the catalyst under the operating conditions was also tested using recovered and recalcined catalysts over three reaction cycles. The highest amount of H<sub>2</sub> was 25 mol% obtained at 450 °C, using 2 g of NiFe<sub>2</sub>O<sub>4</sub> catalyst. The H<sub>2</sub> mol% was enhanced by 45% when compared to the non-catalytic test, showing the catalytic activity of NiFe<sub>2</sub>O<sub>4</sub> catalyst in the WGS and the steam reforming reactions. After the third reaction cycle, the results of XRD demonstrated formation of coke which caused the deactivation of the NiFe<sub>2</sub>O<sub>4</sub> and consequently, a 13.6% reduction in H<sub>2</sub> mol% and a 5.6% reduction in biomass conversion.

**Keywords:** catalytic gasification; supercritical water; hydrogen production; nickel iron oxide; recycling tests

## 1. Introduction

Hydrogen gas is an excellent energy-carrier, which can be combusted directly or used in fuel cells without any direct carbon emissions. Free molecular hydrogen does not occur on Earth and has to be produced from steam reforming of petroleum hydrocarbons or natural gas and the electrolysis of water. Biomass gasification can also be a source of hydrogen but the presence of tar in the syngas is a major problem in conventional process plants. An efficient method to produce hydrogen is supercritical

water gasification (SCWG) of biomass, which can lead to less tar formation and a higher hydrogen yield than the conventional gasification process.

The main reactions that lead to hydrogen gas production during gasification include reforming and water–gas shift. One of the advantages of SCWG is that these reactions can occur within the same reactor space, whereas separate reactors are required in conventional gasification. In addition, due to the high pressures associated with SCWG, the large latent heat of water vaporisation is avoided or minimised, which lowers the amount of energy required to maintain the reaction medium, compared to conventional gasification using steam.

Even though the SCWG increases the selectivity of hydrogen production, it still requires expensive high pressure (>300 bar) and temperature (ca. 700 °C) without catalysts [1–3]. Catalytic supercritical water gasification (CSCWG) of biomass is a promising solution to improve the efficiency of the gasification process. The choice of catalyst to gasify lignocellulosic biomass in supercritical water depends on its ability to lower the activation energies involved in the breaking of C–C and C–O bonds in biomass, accelerate the rate of water–gas shift reaction [1,2,4] and maintain its catalytic and structural stability under hydrothermal conditions. Both homogeneous [5–7] and heterogenous catalysts [8–10] have been applied in SCWG of biomass. Homogeneous catalysts such as KOH and NaOH offer enhanced yields and purity of the hydrogen product due to in situ CO<sub>2</sub> capture, which favourably shifts the equilibrium of water–gas shift reaction. However, the use of heterogeneous catalysts may be cheaper as they can offer long-term processing stability and recyclability compared to homogeneous catalysts [1,2,11,12].

Transition metals are commonly used catalysts for CSCWG because they offer high selectivity, high catalytic activity, and high carbon conversion to gas at moderately low temperatures [3,12]. Many researchers have used nickel-based catalysts CSCWG due to their low-cost, high availability, and catalytic activity in conventional biomass gasification. Results from literature show that many nickel-based catalysts can enhance biomass conversion during SCWG. Elliot [13,14] and Walter and Vogel [15] carried out detailed experiments to evaluate the hydrothermal gasification performance of Ni as a catalyst. They found that changes in the chemical and physical structure of Ni catalyst under hydrothermal conditions helped to improve the gasification reactions of biomass. Furusawa et al. [16,17] found that the carbon yield of gas products can increase with the increase in the surface area of Ni metal.

Nickel ferrite (NiFe<sub>2</sub>O<sub>4</sub>) is an oxide with a spinel AB<sub>2</sub>O<sub>4</sub> structure and is commonly used in the microwave industries [18], in electrocatalysis [18,19], as a catalyst or support in some catalytic reactions such as dry reforming of methane and water gas shift [20,21]. Spinel metal oxide particles have been produced using techniques such as the conventional ceramic method, hydrothermal synthesis, sol-gel, and chemical coprecipitation techniques [22–24].

Literature shows that many ferrites have been synthesized via the combustion of metal precursors in different fuels, yielding special structural and morphological properties for different applications [22,25,26]. The combustion method is a simple and fast technique to obtain materials with desirable physical and chemical properties, high thermal stability, and low production costs. Efficient crystal formation, producing high purity and chemically homogenous powders often consisting of nanosized ferrite particles, may be obtained [25,26]. One major problem of using a solid catalyst to directly convert solid biomass is that the recovery of catalyst from the reaction residues may be costly and troublesome, especially for catalysts with poor hydrothermal stability.

Our previous work [27] focused on a simple evaluation of the effect of NiFe<sub>2</sub>O<sub>4</sub> catalyst on the yields and composition of products from the SCWG of biomass. This present work focuses on understanding the structure-property relationships of the NiFe<sub>2</sub>O<sub>4</sub> catalyst during SCWG by detailed evaluation of the synthesis, characterisation and recycling of the catalyst as well as the detailed characterisation of the gas, liquid, and solid reaction products. In particular, the study of the solid reaction products and the recyclability of the catalysts through its recovery, recalcination and reuse, will help to understand the catalytic mechanism and the potential causes of deactivation of NiFe<sub>2</sub>O<sub>4</sub>

during SCWG of biomass. Such sets of data will be important for further optimisation of the catalyst and the catalytic process in future.

## 2. Experimental

### 2.1. Material

Eucalyptus wood chips, with an approximate 30% moisture content and average particle size of 710  $\mu\text{m}$ , were used as biomass feed material. The biomass was characterised before use. The methodologies of all the analyses to characterize the biomass have been discussed in an earlier paper [28].

### 2.2. Synthesis and Characterization of Catalyst

Nanopowders of nickel ferrite,  $\text{NiFe}_2\text{O}_4$ , were prepared by combustion reaction using ferric nitrate  $\text{Fe}(\text{NO}_3)_3 \cdot 9\text{H}_2\text{O}$ , nickel nitrate  $\text{Ni}(\text{NO}_3)_2 \cdot 6\text{H}_2\text{O}$ , as precursors and urea  $\text{CO}(\text{NH}_2)_2$  as fuel. Stoichiometric amounts of metal nitrates and urea were calculated using the total oxidizing and reducing valences of the components which serve as the numerical coefficients for the stoichiometric balance (Equation (1)), according to the concepts of propellant chemistry [25,26,28,29].

The combustion reaction can be represented as follows:



The measured quantities of the reagents were placed in a vitreous silica basin, homogenized and put into a muffle furnace which was heated rapidly at a rate of  $20\text{ }^\circ\text{C min}^{-1}$  to  $480\text{ }^\circ\text{C}$  until ignition took place, producing a nickel ferrite in a foam form. Thereafter, the material obtained was maintained at  $480\text{ }^\circ\text{C}$  for an additional 20 min to eliminate any volatile product.

The catalyst obtained was characterized by X-ray diffraction Shimadzu 6000 diffractometer,  $\text{Cu K}\alpha$  with a Ni filter and scanning rate of  $2^\circ\text{ }2\theta/\text{min}$ , in a  $2\theta$  range of  $5\text{--}80^\circ$ , the average crystallite sizes were calculated from X-ray line broadening  $d(311)$  using Scherrer's equation [30]. COD (Crystallography Open Database) and ICSD (Inorganic Crystal Structure Database) databases were used for the identification of the phases and the semi-quantitative analyses were carried out using the X'Pert HighScore<sup>TM</sup> software [31].  $\text{N}_2$  adsorption and desorption isotherms of the catalysts were conducted at  $-196.15\text{ }^\circ\text{C}$  in a Micromeritics ASAP 2020 system. The specific surface area was calculated from the  $\text{N}_2$  physical adsorption data using the equation by Brunauer, Emmett, and Teller (BET) [32] and the Barrett-Joyner-Halenda (BJH) was used to determine the pore volume. The reducibility of the sample was examined by temperature programmed reduction (TPR) which was performed in the temperature range of  $25\text{--}1000\text{ }^\circ\text{C}$ , at a heating rate of  $10\text{ }^\circ\text{C min}^{-1}$ , using a Micromeritics 2720 system with a thermal conductivity detector (TCD) to monitor  $\text{H}_2$  consumption. The morphology of the product particle was studied using scanning electron microscopy (SEM) on a Philips XL-30 FEG. Before analysis, the sample was sprayed by sputter-coating with a layer of 30 nm gold using a quorum Q150RS. The acceleration voltage used was 10 kV. The products were further characterized by transmission electron microscopy (TEM) with a Jeol 1200EX Bio at an accelerating voltage of 80 kV. Thermogravimetric analysis (TG) analyses were carried out in a Shimadzu H-50 system. Coke deposition on the catalyst after SCWG tests was examined using the same TG equipment by heating approximately 15 mg of reaction solid residue at a rate of  $10\text{ }^\circ\text{C min}^{-1}$  from  $25$  to  $1000\text{ }^\circ\text{C}$  under an air flux ( $50\text{ mL min}^{-1}$ ). Both TG and derivative thermogravimetry (DTG) curves were obtained.

### 2.3. Catalytic SCWG Test with $\text{NiFe}_2\text{O}_4$

The catalytic activity of the prepared  $\text{NiFe}_2\text{O}_4$  catalyst was examined as a function of reaction temperature ( $400$ ,  $450$ , and  $500\text{ }^\circ\text{C}$ ), using  $0.0$ ,  $1.0$ , and  $2.0\text{ g}$  catalyst, for the SCWG of eucalyptus wood

chips in a batch reactor [27]. A schematic diagram of the 75 cm<sup>3</sup> non-stirred batch reactor is shown in Figure 1. The reactor, made by Hastelloy, was designed to operate up to 600 °C and 45 MPa.

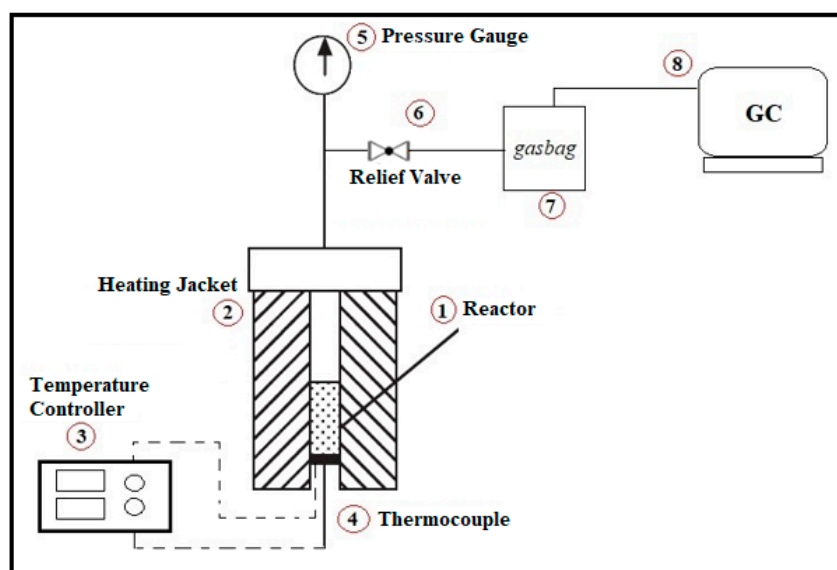


Figure 1. Schematic diagram of batch reactor assembly.

For each experiment, about 2.2 g ( $m_1$ ) of eucalyptus wood chips were loaded into the reactor containing distilled water (20 mL), and then the catalyst was loaded (1.0 g or 2.0 g). The reactor was sealed and heated rapidly at a rate of 20 °C min<sup>-1</sup> up to 450 or 500 °C. Once the reaction temperature was reached, the system was held for a further 60 min. At the end of the reaction time, the reactor was withdrawn from the heater and quickly cooled to ambient temperature with compressed air. After cooling to ambient temperature, the gas product was sampled into a gas-tight 5 mL Tedlar bag for off-line analysis. The compositions of the gas products were determined by injecting 1 ml of gas sample into a Shimadzu GC-2014 gas chromatograph (GC) equipped with both thermal conductivity detector (TCD) and a flame ionisation detector (FID), for the permanent gases (H<sub>2</sub>, O<sub>2</sub>, N<sub>2</sub>, CO, and CO<sub>2</sub>) and hydrocarbon gases, respectively. The permanent gases were separated in a 60–80 mesh packed molecular sieve column (2 m × 2 mm ID) while the hydrocarbons and CO<sub>2</sub> were separated on an 80–100 mesh Hayesep column. Each analysis was carried out twice and the averages were reported.

Semi-quantitative analyses of the liquid products were performed according to a method reported in literature [33,34], as a preliminary analysis to indicate the concentrations of components in the liquid organic products. The area % of each identified compound was expressed as a percentage of the total area of selected peaks in the GC-MS. The method used in this analysis has been discussed in an earlier paper [27]. It was chosen because it was a fast way of obtaining enough information on the components of the liquid phase, which was not the focus of this present research.

The carbon balance was calculated considering the carbon content in the gaseous products, in the solid residue and in the liquid products based on the following equations:

$$\% \text{ carbon}_{(\text{gas phase})} = \frac{\text{mass of carbon in gas components from GC analysis (g)} \times 100}{\text{mass of carbon in eucalyptus wood feed (g)}} \quad (2)$$

$$\% \text{ carbon}_{(\text{solid residue})} = \frac{\text{mass of carbon in char (g)} \times 100}{\text{mass of carbon in eucalyptus wood feed (g)}} \quad (3)$$

$$m_{(\text{char})} = m_{\text{solid residue}} - m_{\text{catalyst}} - m_{\text{ash}} \quad (4)$$

Assuming a 100% balance, the carbon content in the liquid phase was calculated by the difference:

$$\% \text{ carbon (liquid phase)} = 100 - (\text{carbon (gas)} + \text{carbon (solid residue)}) \quad (5)$$

The reaction residue was recovered by vacuum filtration and dried in a vacuum oven at 105 °C for 2 h to a constant weight. The weight of the dried reaction residue containing used catalyst and char, was designated as  $m_2$ . A portion of the dried residue ( $m_3$ ) was heated in a muffle furnace at 500 °C for 2 h to a constant weight to determine the amount of recovered catalyst ( $m_4$ ). After this, the amount of biomass residue ( $m_5$ ), corresponding to the reaction residue, was determined as the difference  $m_5 = m_3 - m_4$ . This amount of char ( $m_5$ ) was adjusted based on the portion of dried residue taken to obtain the total char produced ( $m_5^*$ ). For the recycling procedure, the used catalyst was regenerated by recalcination at 500 °C for 2 h, over two cycles without the use of any solvent to extract the adsorbed organic matter from the catalyst before reuse.

The catalytic activity of the studied  $\text{NiFe}_2\text{O}_4$  was evaluated in terms of biomass conversion to liquid and gases (C), calculated by (Equation (6)).

$$\text{Biomass conversion (C) [\%]} = \frac{(m_1 - m_5^*)}{m_1} \times 100 \quad (6)$$

In addition, the biomass gasification was evaluated separately based on the mass of gas products as follows:

$$\text{Biomass gasification (G) [\%]} = \frac{\sum \left( \frac{P_i \times V \times M_i}{RT} \right)}{m_1} \times 100 \quad (7)$$

where,  $P_i$  = partial pressure of cooled gas component  $i$  at ambient temperature in Pa;  $V$  = volume of reactor headspace in  $\text{m}^3$ ;  $M_i$  = molecular weight of gas component  $i$  in g/mol;  $R$  = gas constant (8.314 J/(mol.K) and  $T$  = ambient temperature in K.

$$\text{Molar composition of gas component } i, x_i [\%] = \frac{n_i}{n_{\text{total}}} \times 100 \quad (8)$$

where,  $n_i$  = moles of gas component  $i$  and  $n_{\text{total}}$  = sum of moles of all gas component.

The catalyst reused was characterised by XRD to learn more about the deactivation mechanism of the nickel ferrite catalyst.

### 3. Results and Discussion

#### 3.1. Characterization of the Fresh Catalyst

The XRD patterns of the fresh  $\text{NiFe}_2\text{O}_4$  powder correspond to the characteristic peaks of the cubic spinel-phase  $\text{NiFe}_2\text{O}_4$  (PDF 96-591-0065).  $\text{Fe}_2\text{O}_3$  (PDF 96-153-2121) and  $\text{NiO}$  (PDF 91-152-6381) were also identified, indicating that the reaction was not complete in the used synthesis conditions. The presence of the secondary phases,  $\text{NiO}$  and  $\text{Fe}_2\text{O}_3$ , revealed by XRD analysis indicated that the reaction was not complete in the used synthesis conditions. It is known that the temperature and fuel effects have strong influence on purity, size, structural, and magnetic properties of materials prepared by combustion route [35,36]. This may be due to the type of fuel, differences in stoichiometry, and component solubility in the inverse spinel of nickel ferrite under the synthesis conditions. The crystallite size of  $\text{NiFe}_2\text{O}_4$ , calculated using Scherrer's equation [30] from lined (311) ( $2\theta = 35.6^\circ$ ) broadening, was 18.11 nm.

The TG analysis of the fresh  $\text{NiFe}_2\text{O}_4$  powder showed a mass loss of 1.95%, indicating high thermal stability. The mass loss was attributed to the loss of precursor residues and water.

The  $\text{H}_2$ -TPR profiles were obtained to investigate how the fresh  $\text{NiFe}_2\text{O}_4$  catalyst would change under reducing environments, e.g., in the presence of hydrogen produced during SCWG in a batch reactor. Results showed that the solid was progressively reduced from 300 to 900 °C (Figure 2), with two

main peaks centred at 360 and 536 °C, which encompass several superimposed reduction events, and a small peak starting around 800 °C. The area of the second peak, at 536 °C, was nearly twice that of the first, at 360 °C. The first peak centered at 360 °C may be interpreted as the overlap of the reduction of NiO → Ni, usually occurring at 330–420 °C [37]. The reduction of bulk Fe<sub>2</sub>O<sub>3</sub> usually occurs in two steps, namely, the phase transformation of Fe<sub>2</sub>O<sub>3</sub> → Fe<sub>3</sub>O<sub>4</sub>, at 471 °C and a broad peak along with a shoulder occurring at T<sub>M</sub> = 651 and 755 °C, respectively, which corresponds to the subsequent reduction of magnetite, ultimately involving the slow phase transformation Fe<sub>3</sub>O<sub>4</sub> → α-Fe [38,39].

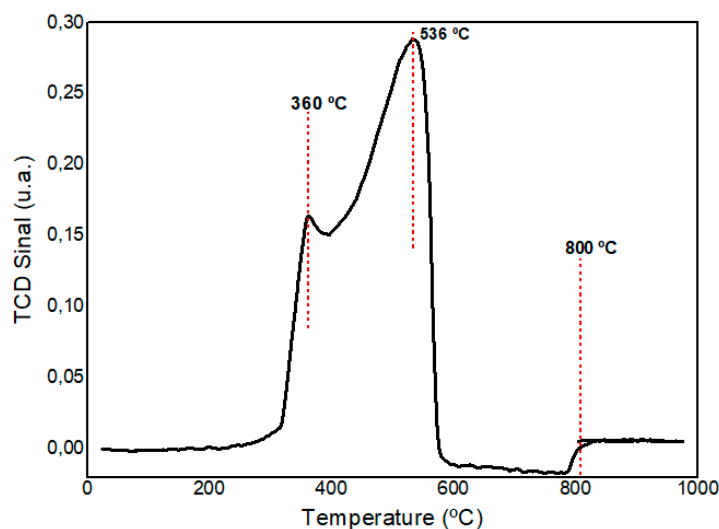
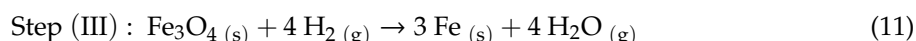
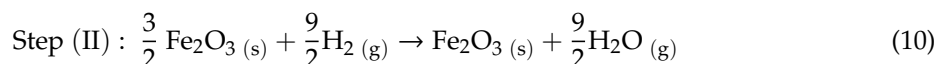
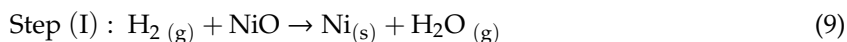


Figure 2. H<sub>2</sub>-TPR profile of fresh NiFe<sub>2</sub>O<sub>4</sub> catalyst.

The two first peaks could correspond to the following reactions [23,24]:



The reduction of NiFe<sub>2</sub>O<sub>4</sub> catalyst shown in Figure 2 is shifted toward lower temperatures, indicating that the presence of nickel facilitated the reduction of iron oxides. However, the spinel phase could not be reduced at a temperature below 900 °C, as confirmed by the integration of the reduction peak areas, so that the peak starting at 800 °C may indicate the initial stages of the NiFe<sub>2</sub>O<sub>4</sub> spinel reduction.

The specific surface area (S<sub>BET</sub>) and the pore volume of the prepared powder were 32.7 m<sup>2</sup> g<sup>-1</sup> and 0.15 cm<sup>3</sup> g<sup>-1</sup>, respectively. The N<sub>2</sub> adsorption/desorption isotherms of the NiFe<sub>2</sub>O<sub>4</sub> powder, shown in Figure 3, are classified as type V, which can be attributed to the weak adsorbent-adsorbate interactions, typically observed on mesoporous materials. A H1 hysteresis loop can be observed, which is characteristic of solids with uniform pore sizes and shapes [40]. The mesoporosity of the synthesized NiFe<sub>2</sub>O<sub>4</sub> is due to the release of gases during the combustion reaction, which leads to the formation of mesopores at the expense of the smaller pores [26,40].

A scanning electron microscope (SEM) was used to observe the morphological aspects of NiFe<sub>2</sub>O<sub>4</sub> powder. The results obtained by SEM (Figure 4a) also showed the formation of agglomerate particles with the shape of irregular porous blocks, consisting of fine particles that easily de-agglomerated. There was also a large particle size distribution from less than 1 μm to greater than 10 μm.

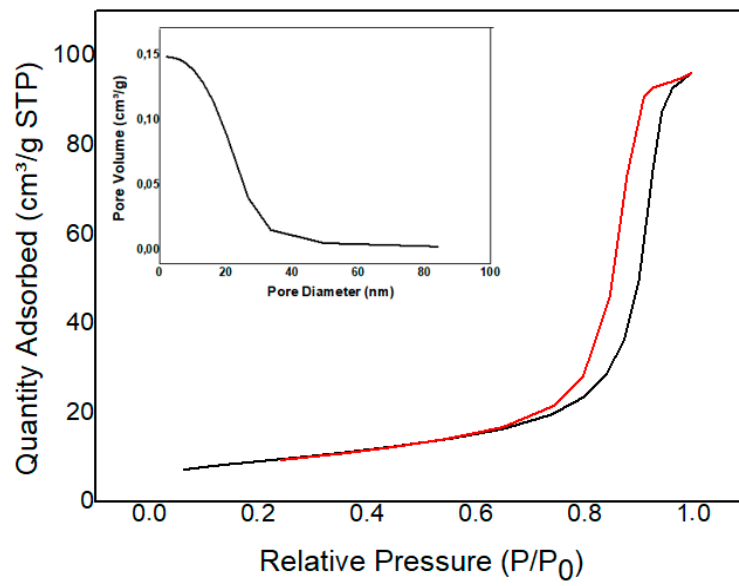


Figure 3. N<sub>2</sub> adsorption/desorption of NiFe<sub>2</sub>O<sub>4</sub>.

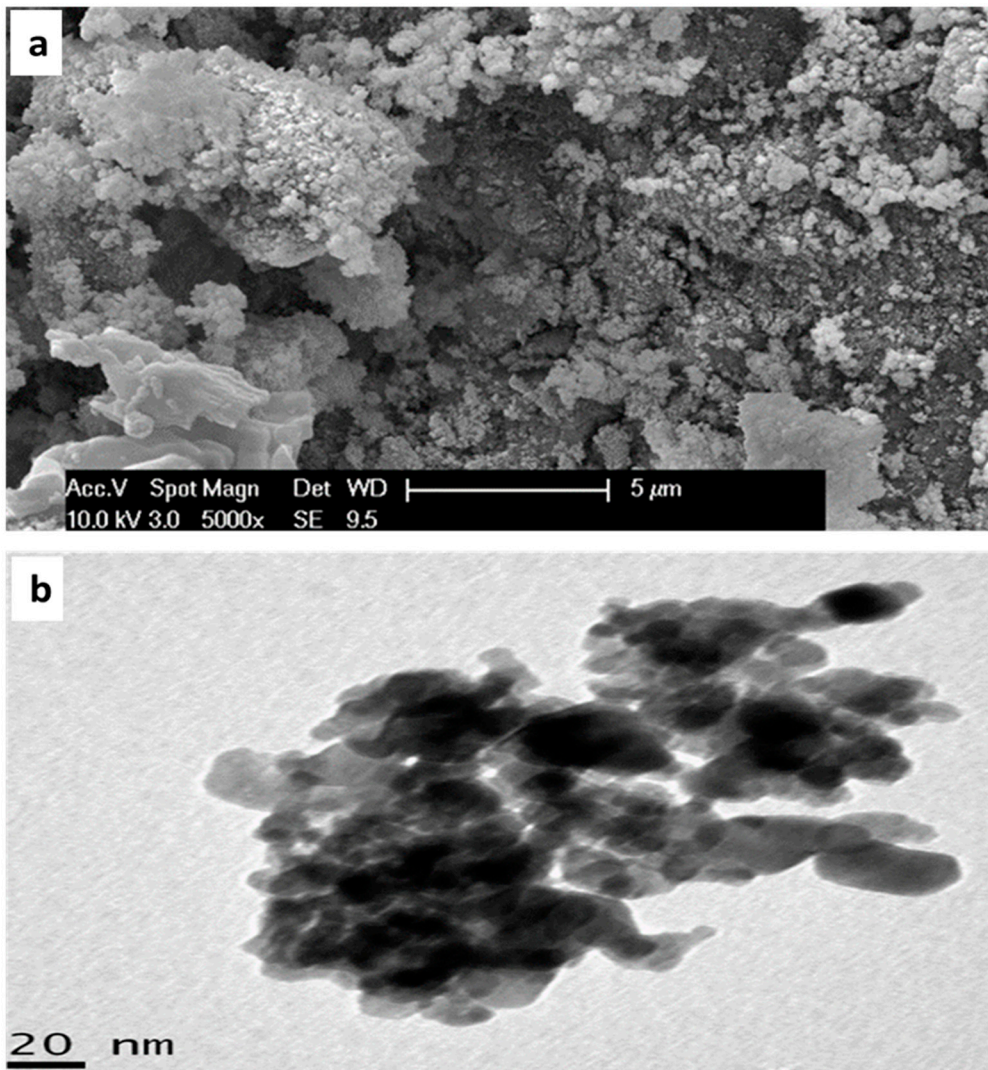


Figure 4. Micrographs of fresh NiFe<sub>2</sub>O<sub>4</sub> (a) scanning electron microscopy (SEM) and (b) transmission electron microscopy (TEM).

In Figure 4a, the presence of small agglomerates with porous aspects can be seen on the surface of a larger agglomerate and this is characteristic of easily de-agglomerated materials. This is due to the high temperatures attained by the combustion reaction during the synthesis of the catalyst, leading to agglomerated nanometric particles [22]. The pores formed by the release of gases during the combustion synthesis and the formation of spherical and agglomerated particles may also be observed.

The transmission electron microscopy (TEM) micrograph (Figure 4b) also shows that the nickel ferrite is formed by agglomerated nanometric particles which tend to react with each other, which reduces the surface energy, forming agglomerates that are easy to de-agglomerate [25]. The transmission electron microscope allows the electron beam to pass through the sample and thus it is possible to better visualize the sizes of the particles. The particle sizes observed by TEM (16–24 nm) are close to those calculated by Scherrer's equation (18.11 nm). This range of values is similar to those previously reported by Costa et al. [22] and Chen and He [41], who obtained a range from 22–29 nm to 5–30 nm, respectively, for nickel ferrite.

### 3.2. Catalytic testing of $\text{NiFe}_2\text{O}_4$ for SCWG of *Eucalyptus* Chips

The results of reaction run and the corresponding conversion of eucalyptus wood chips under SCWG are shown in Table 1. They indicate that the use of the  $\text{NiFe}_2\text{O}_4$  catalyst favoured biomass conversion, which increased with the catalyst loading. The biomass conversion increased with the reaction temperature, from 400 to 450 °C, however, no significant conversion increase was observed at 450 and 500 °C, at constant residence time and catalyst loading. In order to evaluate the effect of the catalyst loading on the SCWG of eucalyptus wood chips, experiments were carried out with different amounts of  $\text{NiFe}_2\text{O}_4$  catalyst (1 or 2 g) at 450 °C, while the residence time was kept constant at 60 min, and the results are shown in Figure 5. For each experiment, the initial theoretical pressure of the reactor at room temperature was read as 0 MPa from a pressure gauge. The  $\text{NiFe}_2\text{O}_4$  catalyst was not previously activated prior to being used in the reactor. In order to investigate the temperature effect on the % mol of the  $\text{H}_2$  gas, the experiments were also performed at 400 and 500 °C, as shown in Figure 6.

**Table 1.** Catalytic supercritical water gasification (CSCWG) testing and biomass conversion using a reaction time of 60 min.

Exp.	Temperature (°C)	Eucalyptus Wood Chips (g)	Catalyst (g)	Biomass Conversion (%)
Test 1	400	2.223	1.998	81.09
Test 2		2.216	-	72.73
Test 3	450	2.199	1.001	84.93
Test 4		2.201	2.005	95.49
Test 5		2.198	-	73.09
Test 6	500	2.207	0.999	85.23
Test 7		2.225	1.999	95.56

In general, the presence of the  $\text{NiFe}_2\text{O}_4$  catalyst led to an increase in the conversion of biomass into liquid and mainly gas products. As shown in Figure 5, the conversion of eucalyptus was around 73%, without catalyst, while the conversion was around 95%, with catalyst. A careful look at the results in Figure 5 reveals that by increasing the amount of catalyst to 2 g, with the same temperature and residence time, the yield of solid residue decreased while the yield of gas products increased. As shown in Figure 6, the maximum total gas produced was 65.94% at 500 °C and 60 min in the presence of 2 g of  $\text{NiFe}_2\text{O}_4$ . Although the experiments performed at 500 °C produced the highest amount of gases, the highest amount of hydrogen (around 25 mol%) was obtained by the conversion of eucalyptus wood chips at 450 °C, as shown in Table 2.

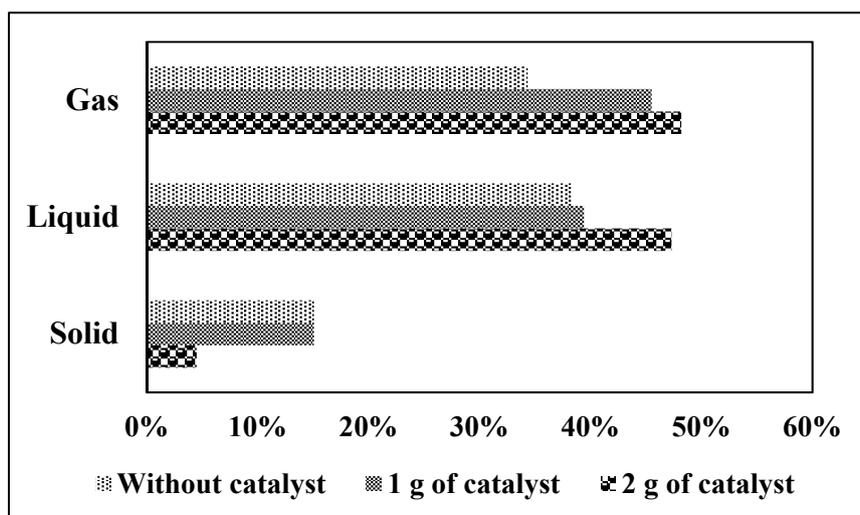


**Figure 5.** Influence of the NiFe<sub>2</sub>O catalyst loading on the carbon balance of supercritical water gasification (SCWG) of eucalyptus wood chips at 450 °C.

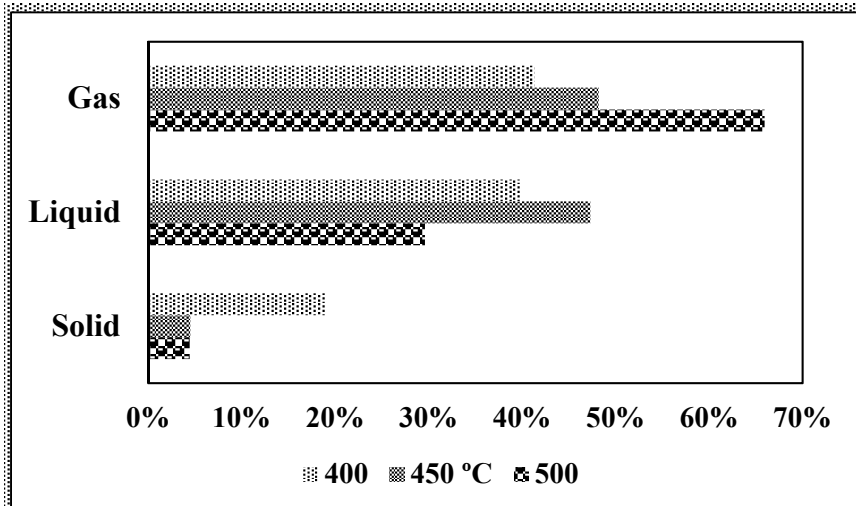


**Figure 6.** Influence of the reaction temperature on the carbon balance of SCWG of eucalyptus wood chips at 400, 450, and 500 °C, using 2 g of NiFe<sub>2</sub>O<sub>4</sub> catalyst and a reaction time of 60 min.

**Table 2.** Composition of the gaseous product.

Exp.	Gas Component (mol%)				
	H <sub>2</sub>	CO	CO <sub>2</sub>	CH <sub>4</sub>	C <sub>2</sub> –C <sub>4</sub>
Test 1	9.52	2.27	75.81	9.15	3.07
Test 2	13.72	6.56	51.85	21.72	5.85
Test 3	18.10	0.70	61.65	14.53	4.85
Test 4	25.05	0.65	56.22	13.55	4.36
Test 5	14.90	2.56	40.83	34.52	7.02
Test 6	19.10	0.50	49.50	24.07	6.47
Test 7	20.19	0.53	49.73	23.11	6.31

The biomass conversion and the percentage of gas products obtained from each experiment can be seen in Tables 1 and 2. It was found that the CSCWG of the eucalyptus wood chips was nearly complete, and the gases at the reactor outlet contained H<sub>2</sub>, CO, CH<sub>4</sub>, CO<sub>2</sub>. As can be seen from Figure 5, the eucalyptus wood chips conversion increased with the increased the amount of catalyst (NiFe<sub>2</sub>O<sub>4</sub>)

with the same temperature and residence time. The maximum biomass conversion of ~95.5% was obtained at 450 °C in the presence of 2 g of NiFe<sub>2</sub>O<sub>4</sub> catalyst and the highest mole fraction of hydrogen was also produced in these conditions, approximately 25 mol%, as it is shown in Table 2. The results showed that the NiFe<sub>2</sub>O<sub>4</sub> catalyst promoted the degradation of eucalyptus wood chips in supercritical water and improved the formation of hydrogen.

One of the main differences between the non-catalytic and catalytic tests was in the concentrations of gas products. Increasing the amount of NiFe<sub>2</sub>O<sub>4</sub> catalyst increased the H<sub>2</sub> gas mol% while reducing the CH<sub>4</sub> gas mol% (Table 2). Increasing the NiFe<sub>2</sub>O<sub>4</sub> loading from 0 to 2 g at 450 °C caused the highest increase of H<sub>2</sub> mol% (45%). Therefore, it can be considered that the NiFe<sub>2</sub>O<sub>4</sub> catalyst favoured the WGS reaction and the steam reforming instead of alternative reaction pathways, as evidenced by the increase in H<sub>2</sub> and CO<sub>2</sub> mol%. These results were consistent with earlier literature reports on CSCWG of biomass using nickel-based catalysts [13–15]. Thus, from the experimental results, NiFe<sub>2</sub>O<sub>4</sub> catalyst also had the capacity to break the C-C and C-O bonds during SCWG, promoting high conversion of biomass into gaseous and liquid products, even at moderate temperatures.

The high conversion of eucalyptus wood chips at 450 and 500 °C indicates that efficient interactions occurred between the NiFe<sub>2</sub>O<sub>4</sub> catalytic surface and reactant the molecules at these temperatures. According to Azadi et al. [42] the use of smaller catalyst particles, as in the present work (18 nm), can reduce the diffusion path and consequently enhance the catalyst performance, as previously reported by other researchers [43–45]. Our results confirmed that the NiFe<sub>2</sub>O<sub>4</sub> powder prepared by the combustion reaction was active as a catalyst for SCWG and may be useful for moderate temperature processes.

During the non-catalytic tests, the influence of temperature was appreciable for the changes in the concentrations of CO, CO<sub>2</sub>, and methane. In going from 450 to 500 °C, the concentration of CO in the gas products decreased by a factor of 2.6, while the concentration on methane increased 1.6 times. The increase in methane concentration could be due to both methanation (exothermic) of carbon oxides (CO<sub>x</sub>) and demethylation (endothermic) of larger molecules in the liquid products. The latter is supported by the overall increase in the biomass gasification at the higher temperature, 500 °C. In the presence of the catalyst, the increase in the overall biomass gasification also showed the influence of the catalyst in converting the liquid and solid products to gases [4,32,43–45].

Table 2 provides good evidence that both the water–gas shift reaction and methane reforming occurred, forming increased concentrations of CO<sub>2</sub> and H<sub>2</sub>. For instance, at 450 °C the molar concentration of CO decreased by at least 89% in the presence of the catalyst compared to non-catalytic tests. At the same time, the concentration of methane fell by at least 30%, when the catalyst was used. At 450 °C, the concentration of H<sub>2</sub> increased by 83% in the presence of 2 g of NiFe<sub>2</sub>O<sub>4</sub> compared to the test without the catalyst. However, for the same amount of catalyst at 500 °C, the CO concentration reduced by 80%, while the methane concentration dropped by 33% compared to tests without the catalyst.

Table 2 also shows that the yield of CO<sub>2</sub> remained consistently high in the presence of catalysts. It is therefore possible to infer that the formation of CO<sub>2</sub> was not only via the water–gas shift reaction but also through the degradation of the biomass. This hypothesis is supported by the results obtained from the GC/MS analysis of the oil products obtained at 450 °C with and without the NiFe<sub>2</sub>O<sub>4</sub> as shown in Figure 7. The bio-oil components have been classified as aliphatic (alcohols, aldehydes, carboxylic acids, and ketones), phenols (phenol, alkylated phenols), alkylbenzenes (xylenes, ethylbenzene, and various methyl benzenes), and polycyclic aromatic hydrocarbons (PAH) (naphthalene and alkylated naphthalenes, biphenyls, fluorene), and others (cyclopropane, cyclopropene, and cycloheptatriene) according to Onwudili and Williams [44].

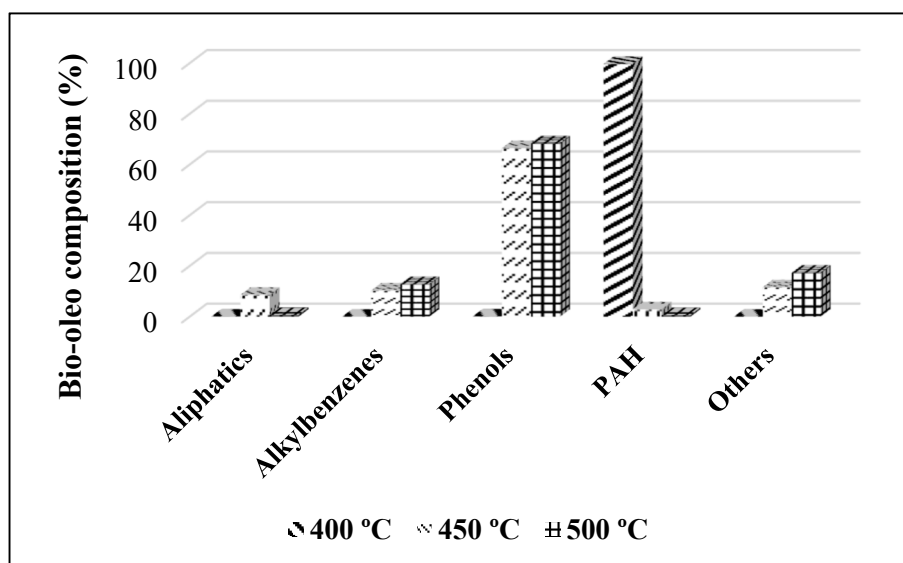


**Figure 7.** Influence of the reaction temperature on the bio-oil products composition of SCWG of eucalyptus wood chips at 400, 450, and 500 °C, using 2 g of NiFe<sub>2</sub>O<sub>4</sub> catalyst and 60 min.

The results showed appreciable formation of cyclic aliphatic and aromatic organic compounds (cyclopropanes, phenols, indenenes, toluene, xylene). These cyclic aromatic compounds are mainly responsible for the formation of tar and coke. These results may indicate that the catalyst was effective in promoting decarboxylation of the biomass or the intermediate liquid products to produce hydrocarbons and CO<sub>2</sub>. The results in Figure 7 also indicate that high amounts of phenolic compounds, such as light alkyl phenols, were obtained at 450 and 500 °C. Complex mixtures of phenolic compounds are usually obtained as products of lignin degradation by flash pyrolysis of lignocellulosic biomass [9,44]. Phenol derivatives are important chemicals and there is a growing interest in producing cost-effective phenols from lignocellulosic materials, such as eucalyptus wood residues.

Clearly, the use of the NiFe<sub>2</sub>O<sub>4</sub> led to a reduction in the yield of biomass residue compared to non-catalytic tests. Moreover, the results show that the yields of char at 450 and 500 °C were similar, decreasing from about 27 wt% to just about 5 wt% in both cases. It can therefore be concluded that the catalyst led to increased conversion of biomass to liquids and gases. Comparing the results obtained using 2 g of catalyst, it could also be observed that biomass residue decreased with temperature. An increase in reaction temperature from 400 to 500 °C led to a reduction of 78.95% (Figure 5). The increase in temperature favoured the gas production and the decomposition of the biomass constituents as residue.

Coke formation by surface polymerization of reaction products, such as phenols, is a common cause of catalyst deactivation. Therefore, the formation of coke was investigated and the thermal curves of the reaction residue, containing biomass residue and catalyst, are shown in Figure 8. TG, DTG and differential thermal analysis (DTA) curves of the solid reaction residues of the Test 4 (450 °C, 2 g of NiFe<sub>2</sub>O<sub>4</sub>) and Test 7 (500 °C, 2 g of NiFe<sub>2</sub>O<sub>4</sub>) are presented and, for comparison, the thermal curves of the fresh catalyst and the eucalyptus are also shown in Figure 8. Two weight losses at T < 500 °C were observed for the raw biomass, while no significant weight loss was observed for the fresh catalyst. The amount of deposited coke can be calculated from the TG curve of used catalysts and varied from 0.03 g (at 450 °C, Test 4) to 0.02 g (at 500 °C, Test 7) and correspond to the weight loss at 450–600 °C in the DTG profile in Figure 8b. The TG analysis of these samples respectively indicated total weight losses of around 26.8% and 11.4%, respectively, mostly related to combustion of residual biomass. The DTG profiles of the two used catalysts (Figure 8b) shows that maximum losses occurred at approximately 420 and 550 °C, and the DTA profiles indicate that they are exothermic events (Figure 8c), since they correspond to the combustion of residual biomass and coke, respectively.

Given the amount of coke deposited on the catalyst, it could be inferred that the deposition of the coke could be the main cause of temporary catalyst deactivation, which hindered further gasification.

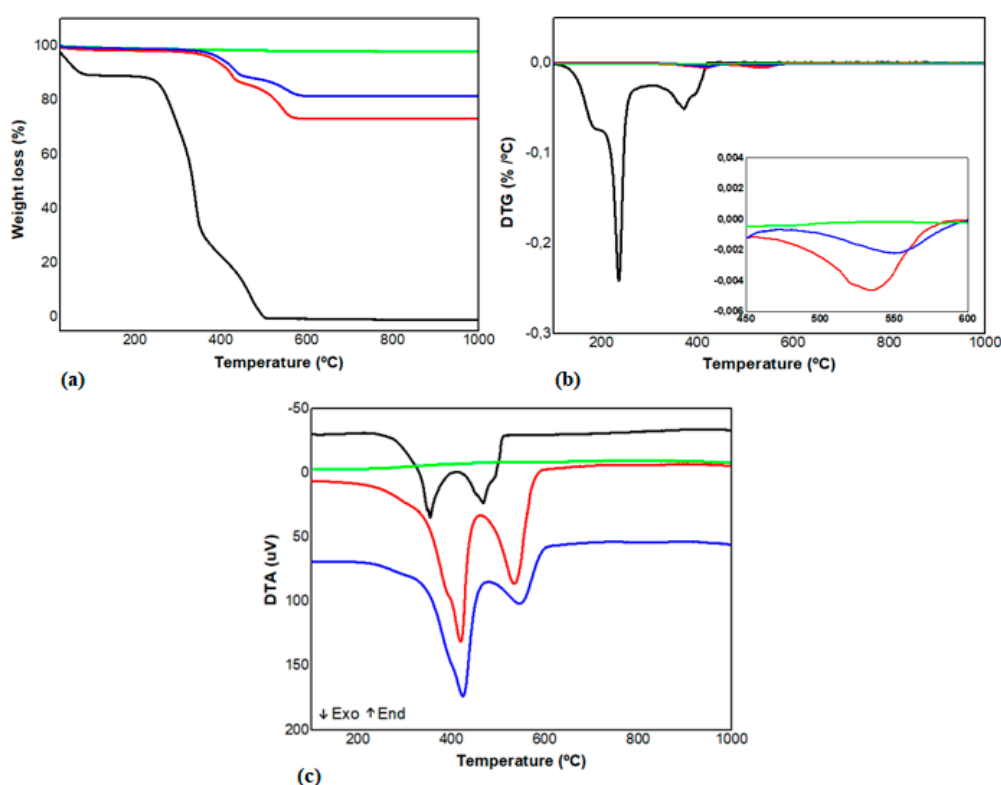


**Figure 8.** TG (a), DTG (b), and DTA (c) curves: — biomass — fresh catalyst — solid reaction residue at 450 °C — solid reaction residue at 500 °C carried out with air.

### 3.3. Catalyst Recycling

To evaluate the recyclability of the  $\text{NiFe}_2\text{O}_4$  catalyst synthesized by combustion reaction, a previously used catalyst was regenerated by calcination in air at 500 °C for 2 h over two recovery cycles. The regenerated catalyst was recovered from tests carried out at 450 °C, 60 min and using 2 g of  $\text{NiFe}_2\text{O}_4$ ; the condition that most favoured hydrogen production. The regenerated catalysts were applied for SCWG of the eucalyptus wood chips under the same conditions for Test 4 in Table 2. The biomass conversion and molar % of the gaseous product for the three reaction cycles are shown in Figure 8.

It can be observed from Figure 9 that the results from the first reaction cycle was equivalent to the previous results obtained under the same conditions (Test 4 in Table 2). However, due to losses during the recovery and calcination procedures, the amount of catalyst used in the recycling tests was 5% less than that used in the first reaction test, and this could have contributed to the drop in the observed conversions. Comparing the results of the first and the third reaction cycles, reductions in biomass conversion (5.6%) and molar % of  $\text{H}_2$  (13.6%) were observed.

The results presented in the Figure 9 show that biomass conversion, biomass gasification, and composition of gas products change slightly with repeated use of the catalysts after each regeneration cycle. Essentially, this could be due to the loss of activity of the catalyst. In addition, based on the data presented in Figure 8, it was possible that the temperature used for recalcination was not enough to guarantee that the catalyst surface was clean.

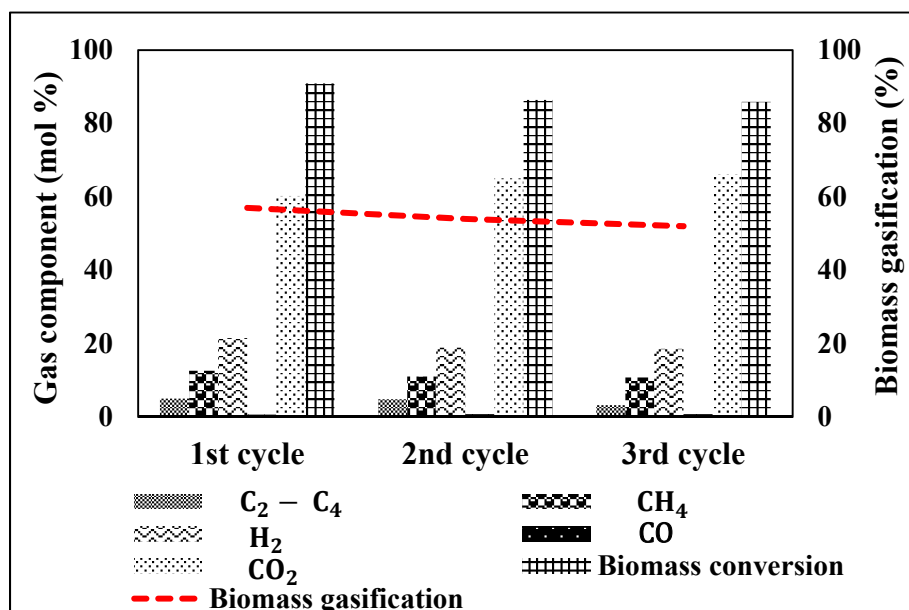


**Figure 9.** Influence of NiFe<sub>2</sub>O<sub>4</sub> recycling on the eucalyptus wood chips SCWG at 450 °C, using 2 g of catalyst and reaction time of 60 min.

Figure 10 shows that the diffraction peaks corresponding to the main phases of catalyst changed after use. The intensity of the NiFe<sub>2</sub>O<sub>4</sub> spinel peaks increased, suggesting that the synthesis of NiFe<sub>2</sub>O<sub>4</sub> continued after the SCWG and regeneration procedure. This result is in agreement with the semi-quantitative analysis of the catalyst composition, as it can be seen in Table 3. Correspondingly, Table 3 also shows the decrease in both the NiO and Fe<sub>2</sub>O<sub>3</sub> percentages, suggesting that NiFe<sub>2</sub>O<sub>4</sub> continued to be formed at the expenses of NiO and Fe<sub>2</sub>O<sub>3</sub>, during the calcination at 500 °C carried out for coke removal. In addition, the crystallite size of NiFe<sub>2</sub>O<sub>4</sub> progressively increased after each use, which suggests that the catalyst deactivation had occurred by sintering [46].

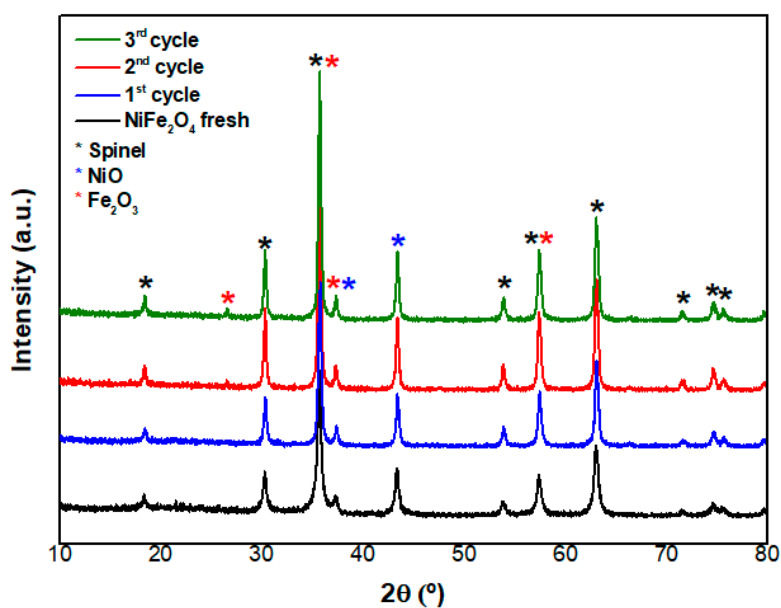


**Figure 10.** XRD patterns of fresh and recycled NiFe<sub>2</sub>O<sub>4</sub> catalysts.

**Table 3.** Semi-quantitative composition\* and NiFe<sub>2</sub>O<sub>4</sub> crystallite size of fresh and recycled catalysts.

Phase	Sample			
	NiFe <sub>2</sub> O <sub>4</sub>			
	Fresh	1st Cycle	2nd Cycle	3rd Cycle
NiFe <sub>2</sub> O <sub>4</sub>	38.6	45.5	48.5	51.0
NiO	33.7	32.7	32.3	30.0
Fe <sub>2</sub> O <sub>3</sub>	27.7	21.8	19.2	19.0
<b>NiFe<sub>2</sub>O<sub>4</sub> Crystallite Size (nm)</b>	18.11	23.18	26.73	28.09

\* Using X'Pert HighScore™.

The diffraction peak corresponding to graphite ( $2\theta = 26.7^\circ$ ) [47], albeit with a low intensity, was detected in the XRD patterns after the third reaction cycle. The formation of coke on the surface of the NiFe<sub>2</sub>O<sub>4</sub> catalyst, would explain the reduction in biomass gasification. It could therefore be concluded that the deactivation of the NiFe<sub>2</sub>O<sub>4</sub> catalyst occurred due to the formation of coke and by the progressive increase in the crystallite size of the NiFe<sub>2</sub>O<sub>4</sub> catalyst, as it can be seen from the results shown in Figure 10 and Table 3. As it was shown in Figure 8, the recalcination temperature was not high enough to remove all the biomass residue on the catalyst surface. This could also be a reason for the reduction in biomass gasification.

#### 4. Conclusions

NiFe<sub>2</sub>O<sub>4</sub> nanoparticles were synthesised and used as catalyst for hydrogen production by supercritical water gasification of eucalyptus wood chips. The catalyst was prepared by the combustion reaction method and a mixture of oxides containing NiFe<sub>2</sub>O<sub>4</sub>, Fe<sub>2</sub>O<sub>3</sub>, and NiO was obtained, indicating that the reaction was not complete in the synthesis conditions used. The catalytic conversion of eucalyptus attained 95%, compared to 73% in the non-catalytic reaction. The maximum biomass gasification was 65.94% at 500 °C and 60 min in the presence of 2 g of NiFe<sub>2</sub>O<sub>4</sub>. The H<sub>2</sub> mol% was enhanced by 45% when compared to the non-catalytic test at 450 °C, showing the catalytic activity of NiFe<sub>2</sub>O<sub>4</sub> in the WGS and the steam reforming reactions, evidenced by the increase in H<sub>2</sub> and CO<sub>2</sub> mol%. The catalyst was effective in promoting decarboxylation of the biomass and of the intermediate liquid products to produce hydrocarbons and CO<sub>2</sub> and produced valuable bio-oil compound such as phenol derivatives. The H<sub>2</sub> mol% reduced after the second reaction cycle. The XRD results demonstrated coke deposition after the third reaction cycle and a progressive increase in the crystallite size of the NiFe<sub>2</sub>O<sub>4</sub> catalyst, which may be the reasons for its deactivation. However, a minimum biomass conversion of 85.90% was obtained after the third reaction cycle, demonstrating a good stability of the catalyst.

**Author Contributions:** Conceptualization, A.C.P.B., J.A.O. and H.A.; methodology, A.C.P.B., J.A.O. and H.A.; formal analysis, A.C.P.B., J.A.O. and H.A.; investigation, A.C.P.B., J.A.O., H.A. and A.I.; resources, J.A.O., H.A., C.A., A.I., S.V.d.M. and E.T.; writing—original draft preparation, A.C.P.B., J.A.O. and H.A.; writing—review and editing, A.C.P.B., J.A.O., H.A., C.A., A.I., S.V.d.M. and E.T.; supervision, J.A.O., H.A., C.A., A.I., S.V.d.M. and E.T. All authors have read and agreed to the published version of the manuscript.

**Funding:** This study was partly financially supported by *Coordenação de Aperfeiçoamento de Pessoal de Nível Superior (CAPES, Brazil)* - Finance Code 23038.002918/2014-75 and the EU Horizon 2020 through the Biofuel Research Infrastructure for Sharing Knowledge 2 (BRSIK2) for A.C.P.B.

**Acknowledgments:** The authors would like to thank the Energy and Bioproducts Research Institute (EBRI), Aston University (UK) and the School of Chemical Engineering, University of Birmingham (UK) for hosting and supporting the researcher (A.C.P.B) during this study.

**Conflicts of Interest:** The authors declare no conflict of interest. The funders had no role in the design of the study; in the collection, analyses, or interpretation of data; in the writing of the manuscript, or in the decision to publish the results.

## References

1. Borges, A.C.P.; Alves, C.T.; Andrade, H.M.C.; Ingram, A.; Vieira de Melo, S.A.B.; Torres, E.A. Supercritical water gasification of Eucalyptus wood chips using  $\text{NiFe}_2\text{O}_4$  as a catalyst. In Proceedings of the ICPRE 2018-3rd International Conference on Power and Renewable Energy, Berlin, Germany, 21–24 September 2018; E3S Web of Conferences. Volume 64, p. 010002. [\[CrossRef\]](#)
2. Rodriguez Correa, C.; Kruse, A. Supercritical water gasification of biomass for hydrogen production—Review. *J. Supercrit. Fluids* **2018**, *133*, 573–590. [\[CrossRef\]](#)
3. Guo, Y.; Wang, S.Z.; Xu, D.H.; Gong, Y.M.; Ma, H.H.; Tang, X.Y. Review of catalytic supercritical water gasification for hydrogen production from biomass. *Renew. Sustain. Energy Rev.* **2010**, *14*, 334–343. [\[CrossRef\]](#)
4. Okalie, J.A.; Rana, R.; Nanda, S.; Dalai, A.K.; Kozinski, J.A. Supercritical water gasification of biomass: A state-of-the-art review of process parameters, reaction mechanisms and catalysis. *Sustain. Energy Fuels* **2019**, *3*, 578–598. [\[CrossRef\]](#)
5. Ding, N.; Azargohar, R.; Dalai, A.K.; Kozinski, J.A. Catalytic gasification of cellulose and pinewood to  $\text{H}_2$  in supercritical water. *Fuel* **2014**, *118*, 416–425. [\[CrossRef\]](#)
6. Sheikhdavoodi, M.J.; Almassi, M.; Ebrahimi-Nik, M.; Kruse, A.; Bahrami, H. Gasification of sugarcane bagasse in supercritical water; evaluation of alkali catalysts for maximum hydrogen production. *J. Energy Inst.* **2015**, *88*, 450–458. [\[CrossRef\]](#)
7. Ge, Z.; Jin, H.; Guo, L. Hydrogen production by catalytic gasification of coal in supercritical water with alkaline catalysts: Explore the way to complete gasification of coal. *Int. J. Hydrog. Energy* **2014**, *39*, 19583–19592. [\[CrossRef\]](#)
8. Yoshida, T.; Oshima, Y.; Matsumura, Y. Gasification of Biomass Model Compounds and Real Biomass in Supercritical Water. *Biomass Bioenergy* **2004**, *26*, 71–78. [\[CrossRef\]](#)
9. Sealock, L.J., Jr.; Elliott, D.C. Method for the Catalytic Conversion of Lignocellulosic Materials. U.S. Patent 5,019,135, 28 May 1991.
10. Yamaguchi, A.; Hiyoshi, N.; Sato, O.; KBando, K.; Osada, M.; Shirai, M. Hydrogen production from woody biomass over supported metal catalysts in supercritical water. *Catal. Today* **2009**, *146*, 192–195. [\[CrossRef\]](#)
11. Lu, Y.; Li, S.; Guo, L. Chapter 13: Catalysis in Supercritical Water Gasification of Biomass: Status and Prospects. In *Near-Critical and Supercritical Water and Their Applications for Biorefineries, Biofuels and Biorefineries*, 2nd ed.; Fang, Z., Xu, C., Eds.; Springer-Science+Business Media Dordrecht: New York, NY, USA; London, UK, 2014.
12. Li, S.; Guo, L. Stability and activity of a co-precipitated Mg promoted Ni/ $\text{Al}_2\text{O}_3$  catalyst for supercritical water gasification of biomass. *Int. J. Hydrog. Energy* **2019**, *44*, 15842–15852. [\[CrossRef\]](#)
13. Elliot, D.C. Catalytic hydrothermal gasification of biomass. *Biofuels Bioprod. Biorefin.* **2008**, *2*, 254–265. [\[CrossRef\]](#)
14. Elliot, D.C.; Sealock, L.J., Jr.; Baker, E.G. Chemical processing in high-pressure aqueous environments. Development of catalyst for gasification. *Ind. Eng. Chem. Res.* **1993**, *32*, 1542–1548. [\[CrossRef\]](#)
15. Waldner, M.H.; Vogel, F. Renewable production of methane from woody biomass by catalytic hydrothermal gasification. *Ind. Eng. Chem. Res.* **2005**, *44*, 4543–4551. [\[CrossRef\]](#)
16. Furusawa, T.; Sato, T.; Saito, M.; Ishiyama, Y.; Sato, M.; Itoh, N.; Suzuki, N. The evaluation of the stability of Ni/MgO catalysts for the gasification of lignin in supercritical water. *Appl. Catal. A Gen.* **2007**, *327*, 300–310. [\[CrossRef\]](#)
17. Furusawa, T.; Sato, T.; Sugito, H.; Miura, Y.; Ishiyama, Y.; Sato, M.; Itonh, N.; Suzuki, N. Hydrogen production from the gasification of lignin with nickel catalysts in supercritical water. *Int. J. Hydrog. Energy* **2007**, *32*, 699–704. [\[CrossRef\]](#)
18. Maltha, A.; Kist, H.F.; Brunet, B.; Ziolkwski, J.; Onishi, H.; Iwasawa, Y.; Ponec, V. The sites of manganese-and-cobalt containing catalysts in the seletive gas phase reduction of nitrobenzene. *J. Catal.* **1994**, *149*, 356–363. [\[CrossRef\]](#)
19. Doppler, G.; Trautwein, A.X.; Ziethen, H.M.; Ambach, E.; Lehnert, R.; Sorague, M.; Gonser, U. Physical and catalytic Properties of high-temperature water-gas shift catalysts based upon iron-chromium oxides. *Appl. Catal.* **1988**, *40*, 119–130. [\[CrossRef\]](#)

20. Lelis, M.F.F.; Menini, L.; da Silva, M.J.; Fabris, J.D.; Lago, R.M.; Gusevskwysa, E.V. Novel solvent free liquid-phase oxidation of [beta]-pinene over heterogeneous catalysts based on  $\text{Fe}_{3-x}\text{M}_x\text{O}_4$  (M=Co and Mn). *Appl. Catal. A Gen.* **2004**, *269*, 117–121.
21. Oliveira, L.C.A.; Fabris, J.D.; Rios, R.R.V.A.; Mussel, W.N.; Lago, R.M.  $\text{Fe}_{3-x}\text{M}_x\text{O}_4$  catalysts: Phase transformations and carbon monoxide oxidation. *Appl. Catal. A Gen.* **2004**, *259*, 253–259. [[CrossRef](#)]
22. Costa, A.C.F.M.; Lula, R.T.; Kiminami, R.H.G.A.; Gama, L.F.V.; de Jesus, A.A.; Andrade, H.M.C. Preparation of nanostructured  $\text{NiFe}_2\text{O}_4$  catalysts by combustion reaction. *J. Mater. Sci.* **2005**, *41*, 4871–4875. [[CrossRef](#)]
23. Benrabaa, R.; Lofberg, A.; Caballero, J.G.; Bordes-Richards, E.; Rubbens, A.; Vannier, R.N.; Boukhlof, H.; Barama, A. Sol-gel synthesis and characterization of silica supported nickel ferrite catalysts for dry reforming of methane. *Catal. Commun.* **2015**, *58*, 127–131. [[CrossRef](#)]
24. Pannaparayil, T.; Marande, R.; Komarneni, S.; Sankar, S.G. A novel low-temperature preparation of several ferrimagnetic spinels and their magnetic and Mössbauer characterization. *J. Appl. Phys.* **1988**, *64*, 5641. [[CrossRef](#)]
25. Alves, C.T.; Oliveira, A.; Carneiro, S.A.V.; Silva, A.G.; Andrade, H.M.C.; Vieira de Melo, S.A.B.; Torres, E.A. Transesterification of waste frying oil using a zinc aluminate catalyst. *Fuel Process. Technol.* **2013**, *106*, 102–107. [[CrossRef](#)]
26. Patil, K.C.; Hedge, M.S.; Rattan, T.; Aruna, S.T. *Chemistry of Nanocrystalline Oxide Materials, Combustion Synthesis, Properties and Applications*; Word Scientific Pub: Singapore, 2008.
27. Borges, A.C.P.; Onwuidili, J.A.; Andrade, H.M.C.; Alves, C.T.; Ingram, A.; Vieira de Melo, S.A.B.; Torres, E.A. Catalytic supercritical water gasification of eucalyptus wood chips in a batch Reactor. *Fuel* **2019**, *255*, 115804–115813. [[CrossRef](#)]
28. Borges, A.C.P.; Alves, C.T.; Torres, E.A. Torrefied Eucalyptus Grandis Characterization as a Biomass to Using in Industrial Scale. *Chem. Eng. Trans.* **2016**, *49*, 283–288.
29. González-Cortés, S.L.; Imbert, F.E. Fundamentals, properties and applications of solid catalysts prepared by solution combustion synthesis (SCS). *Appl. Catal. A Gen.* **2013**, *452*, 117–131. [[CrossRef](#)]
30. Klung, H.; Alexander, L. *X-ray Diffraction Procedures*; John Wiley & Sons: New York, NY, USA, 1962; p. 491.
31. Degen, T.; Sadki, M.; Bron, E.; Konig, U.; Nénert, G. *Powder Diffraction*; Cambridge University: Cambridge, UK, 2014; Volume 29, pp. S13–S18.
32. Lloyd, L.; Ridler, D.E.; Twigg, M.V. *Catalyst Handbook*, 2nd ed.; Wolfe: London, UK, 1989; p. 28.
33. Wang, Z.; Shui, H.; Pan, C.; Li, L.; Ren, S.; Lei, Z.; Kang, S.; Wei, C.; Hu, J. Structural characterization of the thermal extracts of lignite. *Fuel Process. Technol.* **2014**, *120*, 8–15. [[CrossRef](#)]
34. Duan, P.; Jin, B.; Xu, Y.; Yang, Y.; Bai, X.; Wang, F. Thermo-chemical conversion of *Chlorella pyrenoidosa* to liquid biofuels. *Bioresour. Technol.* **2013**, *133*, 197–205. [[CrossRef](#)]
35. Prabhakaran, T.; Hemalatha, J. Combustion synthesis and characterization of highly crystalline single phase nickel ferrite nanoparticles. *J. Alloys Compd.* **2011**, *509*, 7071–7077. [[CrossRef](#)]
36. Karakaş, Z.K.; Boncukçuoğlu, R.; Karakaş, I.H. The effects of fuel type in synthesis of  $\text{NiFe}_2\text{O}_4$  nanoparticles by microwave assisted combustion method. *J. Phys. Conf. Ser.* **2016**, *707*, 012046. [[CrossRef](#)]
37. Jones, A.; McNicol, B.; Dekker, M. *Temperature Programmed Reduction for Solid Materials Characterization*; Chemical Industrial Series; CRC Press: Boca Raton, FL, USA, 1986; Volume 24.
38. Venugopal, A.; Scurrall, M.S. Low temperature reductive pretreatment of  $\text{Au/Fe}_2\text{O}_3$  catalysts, TPR/TPO studies and behaviour in the water-gas shift reaction. *Appl. Catal. A* **2004**, *258*, 241–249. [[CrossRef](#)]
39. Jin, Y.; Datye, A.K. Phase transformations in iron Fischer-Tropsch catalysts during temperature-programmed reduction. *J. Catal.* **2000**, *196*, 8–17. [[CrossRef](#)]
40. Thommes, M.; Kaneko, K.; Neimark, A.V.; Olivier, J.P.; Rodriguez-Reinoso, F.; Rouquerol, J.; Sing, K.S.W. Physisorption of gases, with special reference to the evaluation of surface area and pore size distribution (IUPAC Technical Report). *Pure Appl. Chem.* **2015**, *87*, 1051–1069. [[CrossRef](#)]
41. Chen, D.H.; He, X.R. Synthesis of nickel ferrite nanoparticles by sol-gel method. *Mater. Res. Bull.* **2001**, *38*, 1369–1377. [[CrossRef](#)]
42. Azadi, P.; Farnood, R. Review of heterogeneous catalysts for sub- and supercritical water gasification of biomass and wastes. *Fuel Energy Abstr.* **2011**, *36*, 9529–9541. [[CrossRef](#)]
43. Susanti, R.F.; Dianningrum, L.W.; Yum, T.; Kim, Y.; Lee, B.; Kim, J. High-yield hydrogen production from glucose by supercritical water gasification without added catalyst. *Int. J. Hydrog. Energy* **2012**, *37*, 11677–11690. [[CrossRef](#)]

44. Onwuidili, J.A. Supercritical water gasification of RDF and its components over RuO<sub>2</sub>/γ-Al<sub>2</sub>O<sub>3</sub> catalyst: New insights into RuO<sub>2</sub> catalytic reaction mechanisms. *Fuel* **2016**, *181*, 157–169. [[CrossRef](#)]
45. Cortright, R.D.; Davda, R.R.; Dumesic, J.A. Hydrogen from catalytic reforming of biomass-derived hydrocarbons in liquid water. *Nature* **2002**, *418*, 964–967. [[CrossRef](#)]
46. Argyle, M.D.; Bartholomew, C.H. Heterogeneous Catalyst Deactivation and Regeneration: A Review. *Catalysts* **2015**, *5*, 145–269. [[CrossRef](#)]
47. Lu, Y.; Zhu, Y.; Li, S.; Zhang, X.; Guo, L. Behavior of nickel catalysts in supercritical water gasification of glucose: Influence of support. *Biomass Bioenergy* **2014**, *67*, 125–136. [[CrossRef](#)]



© 2020 by the authors. Licensee MDPI, Basel, Switzerland. This article is an open access article distributed under the terms and conditions of the Creative Commons Attribution (CC BY) license (<http://creativecommons.org/licenses/by/4.0/>).